Journal of Thermal Biology 115 (2023) 103625

Contents lists available at ScienceDirect

Journal of Thermal Biology

journal homepage: www.elsevier.com/locate/jtherbio

Assessment of the thermal tissue models for the head and neck hyperthermia treatment planning

Tomas Drizdal [a,b,*], Gerard C. van Rhoon [a], Ondrej Fiser [b], David Vrba [b], Netteke van Holthe [a], Jan Vrba [b], Margarethus M. Paulides [a,c]

[a] Hyperthermia Unit, Dept. of Radiation Oncology, Erasmus MC Cancer Institute, Dr. Molewaterplein, 3015 GD, Rotterdam, Rotterdam, the Netherlands
[b] Dept. of Biomedical Technology, Faculty of Biomedical Engineering, Czech Technical University in Prague, Nam. Sitna 3105, 272 01, Kladno, Czech Republic
[c] Dept. of Electrical Engineering, Eindhoven University of Technology, De Rondom 70, 5612 AP, Eindhoven, the Netherlands

ARTICLE INFO

Keywords:
Hyperthermia
Temperature prediction
Head and neck

ABSTRACT

Purpose: To compare different thermal tissue models for head and neck hyperthermia treatment planning, and to assess the results using predicted and measured applied power data from clinical treatments.
Methods: Three commonly used temperature models from literature were analysed: "constant baseline", "constant thermal stress" and "temperature dependent". Power and phase data of 93 treatments of 20 head and neck patients treated with the HYPERcollar3D applicator were used. The impact on predicted median temperature T50 inside the target region was analysed with maximum allowed temperature of 44 °C in healthy tissue. The robustness of predicted T50 for the three models against the influence of blood perfusion, thermal conductivity and the assumed hotspot temperature level was analysed.
Results: We found an average predicted T50 of 41.0 ± 1.3 °C (constant baseline model), 39.9 ± 1.1 °C (constant thermal stress model) and 41.7 ± 1.1 °C (temperature dependent model). The constant thermal stress model resulted in the best agreement between the predicted power (P = 132.7 ± 45.9 W) and the average power measured during the hyperthermia treatments (P = 129.1 ± 83.0 W).
Conclusion: The temperature dependent model predicts an unrealistically high T50. The power values for the constant thermal stress model, after scaling simulated maximum temperatures to 44 °C, matched best to the average measured powers. We consider this model to be the most appropriate for temperature predictions using the HYPERcollar3D applicator, however further studies are necessary for developing of robust temperature model for tissues during heat stress.

1. Introduction

Hyperthermia treatment (HT), i.e. artificial temperature elevation in range of 40–44 °C for a duration of 60–90 min, proved beneficial when combined with radiotherapy and/or chemotherapy for patients treated with various tumour diseases (Franckena et al., 2008; Issels et al., 2018; Peeters et al., 2022). The temperature increase in deep HT (targets deeper than 5 cm from the patient surface) is usually achieved by applying constructive interference of several electromagnetic (EM) field waves radiated from the antenna elements arranged in the phased array setup surrounding the patient (Kok et al., 2020). The temperature during the HT is generally measured invasively by using temperature probes, which represent a burden for patients. Often only intraluminal probes are available with a doubtful tissue contact and no intra-tumoral information. Moreover, both approaches provide temperature information only from a few measurement locations. Patient specific hyperthermia treatment planning (HTP) has the potential to provide 3D temperature information before and during the HT, but is prone to thermal tissue property inaccuracies (Paulides et al., 2013; Gavazzi et al., 2020; Kok and Crezee, 2021; Kok et al., 2021b). Clinical guidance based on absolute temperature HTP is hampered by uncertain values for (temperature-dependent) tissue cooling (de Greef et al., 2010; 2011).

HTP is being used at Erasmus MC prior to every deep HT to find the optimal amplitude and phase settings for the signals fed to the antennas (Canters et al., 2012). Hereto, we use our in-house visualization tool for electromagnetic dosimetry and optimization, i.e. VEDO for objective

* Corresponding author. Hyperthermia Unit, Dept. of Radiation Oncology, Erasmus MC Cancer Institute, Dr. Molewaterplein, 3015 GD, Rotterdam, Rotterdam, the Netherlands.
E-mail address: t.drizdal@erasmusmc.nl (T. Drizdal).

https://doi.org/10.1016/j.jtherbio.2023.103625
Received 22 August 2022; Received in revised form 9 June 2023; Accepted 9 June 2023
Available online 4 July 2023

treatment guidance based on computer optimization rather than clinical personal experiences (Rijnen et al., 2013). Currently, we base our clinical HTP routine purely on specific absorption rate (SAR) predictions. However, since waterbolus cooling is important especially for H&N hyperthermia, we therefore aim at switching towards temperature based HTP. One of the main rationales for the generally applied SAR based approach is the uncertainty of the tissue temperature parameters and especially of the blood perfusion. Earlier, we showed a crucial impact of the tissue cooling model when performing temperature simulation based applicator selection, for which qualitative temperature predictions were sufficient (Drizdal et al., 2018). When applying constant and temperature dependent blood perfusion models for analysing head and neck (H&N) HT quality, we obtained mean temperature differences up to 2 °C for superficial applicators and 1.6 °C for the HYPERcollar. Notably, a favourable T50 was predicted for the superficial applicators over the HYPERcollar for some patients when using the temperature dependent model. Here, the constant perfusion thermal modelling and SAR analysis consistently showed superiority of the HYPERcollar H&N applicator. A detailed study on the impact of constant and temperature dependent perfusion on HT quality is missing.

The purpose of this study was to assess temperature tissue models and investigate their impact on hyperthermia treatment quality in the H&N region. Hereto, we studied the impact of two constant and one temperature dependent perfusion models available in the literature on the predicted median temperature T50 (°C) achieved in the clinical target volume (CTV). We used data of 20 patients with 93 sessions treated with H&N hyperthermia using the HYPERcollar3D. The clinically applied relative power and phase settings were used to simulate the temperature distribution. Following our clinical protocol, we increased total power to obtain a hotspot in normal tissue, which was assumed to be 44 °C for our simulations. The resultant power levels were compared to the average measured power during treatments. The robustness of our numerical analysis was studied by varying blood perfusion, thermal conductivity and the assumed hotspot temperature. All comparisons were based on the predicted T50, i.e. the median temperature in the CTV.

2. Material and methods

2.1. Patient selection

For this study, we selected the first 20 patients treated with HYPERcollar3D at our clinic between 2014 and 2017. The patients group comprised patients with oropharyngeal tumors (9), neck node metastases (3), affected parotid gland (2), laryngeal tumors (2), one tumour in the oral cavity, a nasopharyngeal tumour, a hypopharyngeal tumour and a tumour in the sinus maxillaris, i.e. 14 males and six females with mean age of 61.7 ± 12 (mean ± one standard deviation) years. The average CTV depth for those 20 patients was 26 ± 13 mm (mean ± one standard deviation).

2.2. Electromagnetic field modelling

An overview of the HTP procedure applied at Erasmus MC Cancer Institute for every H&N patient treated with HYPERcollar3D is shown in Fig. 1. The 3D patient specific model is created using automatic segmentation technique of the CT images followed by manual assignment in iSeg software (v. 3.8, Zürich MedTech AG, Zürich, Switzerland) shown in Fig. 1a) and Fig. 1b) respectively (Verhaart et al., 2014b). It takes about 30 min of computer and 15–30 min of operator time (depending on amount of CT images) to create a 3D patent model consisting up to 15 tissues. The 3D patient model is then imported and positioned inside the HYPERCollar3D model in SEMCAD X program (v. 14.8.6, Speag, Zürich, Switzerland) for electromagnetic field (EM) and temperature simulations, shown in Fig. 1c). The positioning of 3D patient model follows patient position in the real HYPERcollar3D applicator during the HT. A harmonic simulation with 15 periods at 434 MHz consisting typically of 70 million cells using uniform discretization step of 1.25 mm is calculated in up to 15 min using two GTX 1080 graphical processor units for each out of the 20 patch antennas of the HYPERcollar3D. Twelve antennas with the highest average SAR inside the CTV are selected, since 12 amplifiers are available (Togni et al., 2013). Afterwards, particle swarm optimization of amplitude and phase signals of 12

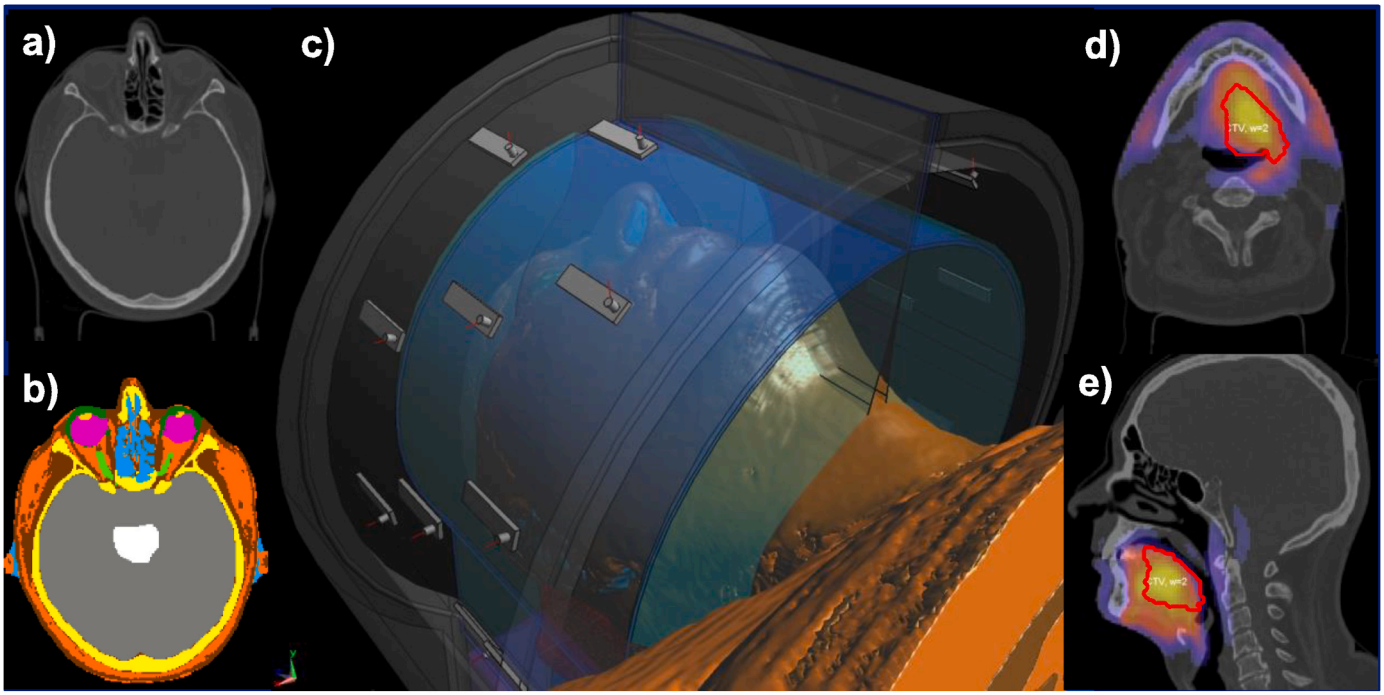

Fig. 1. The overview of the hyperthermia treatment planning procedure for the HYPERCollar3D at the Erasmus MC Cancer Institute. a) CT slice, b) corresponding iSeg segmentation, c) simulation setup including patient and HYPERcollar3D models in SEMCAD X. d) axial and e) sagittal views of an example of SAR coverage image in VEDO. The radiotherapy clinical target volume (CTV) is encircled in red in d) and e).

HYPERcollar3D antennas is applied in order to provide the best possible SAR coverages of the CTV (Chen, 2016). Next to the particle swarm optimization algorithm it is possible also to use other SAR based and thermal optimization techniques (Cappiello et al., 2017; Bellizzi et al., 2019; Kok et al., 2017; Gaffoglio, 2021). Using our in-house developed tool VEDO, the CT and radiotherapy CTV are displayed with the (optimized) SAR results on top (Fig. 1d) and e)). VEDO uses precomputed EM field distributions from individual antennas for online (during the HT) re-optimizations of amplitudes and phases of antennas input signals according to the invasively measured temperatures or patient feedback (Rijnen et al., 2013).

2.3. Thermal modelling

For temperature simulations, we used the power and phase settings from the end of each hyperthermia treatment as these settings are used throughout steady state. This combined SAR was used for temperature simulations calculated according to the Pennes bioheat equation (Pennes, 1948)

$$c\rho\frac{\partial T}{\partial t} = \nabla.(k\nabla T) - SF\rho_b c_b \omega(T - T_b) + \rho SAR + \rho Q$$

where c (J kg^{-1}K^{-1}) represents the specific heat capacity, ρ (kg m^{-3}) the density, k (W m^{-1}K^{-1}) the thermal conductivity, c_b (J kg^{-1}K^{-1}) the specific heat capacity of blood, ω (ml min $^{-1}$kg^{-1}) the blood perfusion rate, Q (W kg^{-1}) the metabolic heat generation, T_b (K) the temperature of the circulated blood. SF (−) is a scaling factor enabling implementation of a temperature dependent blood perfusion model (Drizdal et al., 2010; 2018; Song et al., 1984; Lang et al., 1999). All dielectric and thermal properties except for muscle, fat and tumour used in the simulations were assigned according to Table 1 (Gabriel et al., 1996; Hasgall et al., 2018).

A water temperature of 30 °C (standard temperature in clinical practice) and a heat transfer coefficient of h = 292 Wm^{-2}K^{-1} were used as a default water bolus values for temperature simulations (Drizdal et al., 2021b). Mimicking our common strategy of heating up to patient's tolerance, total power of the HYPERcollar3D was increased, i.e. scaled, in order to obtain maximum of 44 °C in healthy tissue outside the CTV. Even though this temperature might not always be achieved in clinical practise, this approach allows us to compare different perfusion models at a realistic heating levels.

Table 1
Dielectric (@434 MHz (Gabriel et al., 1996)) and thermal (@37 °C (Hasgall et al., 2018)) properties used in the simulations, * represents values from tissue parameter optimization procedure for ten patients treated with the HYPERcollar applicator (Verhaart et al., 2015). Internal air and lung were modelled in temperature simulations using a boundary condition. Following Lang et al. (1999) the value for tumour perfusion at 37 °C is 1.85 times higher than the rest value for muscle perfusion 37 °C.

tissue	ε_r (−)	σ (Sm^{-1})	P (kgm^{-3})	c (J kg^{-1} K^{-1})	k (W m^{-1} K^{-1})	ω (ml min^{-1} kg^{-1})	Q (W kg^{-1})
air	1	0	1.2	–	–	–	–
blood	–	–	1050	3617	–	–	–
bone	13.1	0.09	1908	1312	0.32	10	0.15
brainstem	55.1	1.05	1046	3630	0.51	559	11.4
cartilage	45.1	0.6	1099	3568	0.49	35	0.54
cerebellum	55.1	1.05	1045	3653	0.51	763	15.5
cerebrum	56.8	0.75	1045	3696	0.55	763	15.5
fat	11.6	0.08	911	2348	0.21/ 0.5*	32.7/ 255*	0.51
Lucite	2.6	0.003	1000	–	–	–	–
lung	23.6	0.38	394	–	–	–	–
muscle	56.7	0.8	1090	3421	0.49/ 0.4*	39.1/ 442.8*	0.96
optical nerve	35	0.46	1075	3613	0.49	160	2.5
sclera	57.4	1.01	1032	4200	0.58	380	5.9
spinal cord	69	1.53	1005	4047	0.59	160	2.5
tumour/ GTV	59	0.89	1050	3950	0.51/ 1.5*	72.4/ 848*	0
thyroid	61.3	0.89	1050	3609	0.52	5624	87
vitreous humor	69	1.53	1005	4047	0.59	0	0
water	78	0.04	1000	–	–	–	–

2.4. Temperature cooling modelling

In this study, we considered standard temperature tissue models used for HT temperature predictions.

2.4.1. Constant model 1: constant values at 37 °C

The first constant temperature model ($\omega_{const.,37°C}$) is the standard model based on literature perfusion values at baseline, i.e. 37 °C (Hasgall et al., 2018).

2.4.2. Constant model 2: optimized perfusion and thermal conductivity values

The second constant temperature model ($\omega_{const.,Tstress}$) was obtained by minimizing of the difference between invasively measured and simulated temperature profiles for ten patients (not part of this study) treated with HYPERcollar applicator (Verhaart et al., 2014a; 2015) (values with * in Table 1). We currently consider this model to be the best one for H&N hyperthermia temperature predictions since, to our knowledge, it is the only model where blood perfusion and thermal conductivity were reconstructed 'in-vivo' under the heat stress conditions. However, note that generally higher SAR levels (+50% reported in (Paulides et al., 2016)), and therefore most probably also higher temperatures, are achieved with the HYPERcollar3D compared to previously used HYPERcollar (in use in 2007–2014) applicator (Verduijn et al., 2018).

2.4.3. Temperature dependent blood perfusion and constant conductivity model

As a third considered model, we used the temperature dependent blood perfusion model ($\omega_{T\text{-}dependent}$) in which the blood perfusion of muscle, fat and tumour is changing as a function of actual temperature as shown in Fig. 2. In the blood perfusion model introduced by Song et al. (1984), the temperature decreases after reaching 44–45 °C due to the vasculature shutdown (Lang et al., 1999). Since, in all our temperature simulations, we limited the maximum allowed temperature in

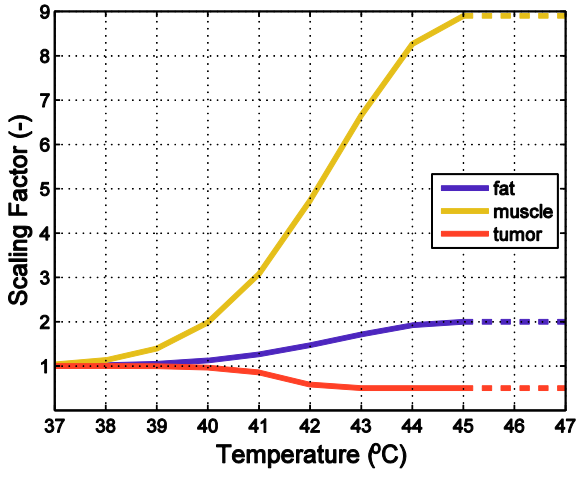

Fig. 2. Temperature dependent blood perfusion scaling factor (SF) for fat, muscle and tumour.

healthy tissues to 44–45 °C, we extrapolated the SF over 45 °C with constant values (represented in Fig. 2 by dotted lines). Our implementation copy the model developed by Lang et al. which is available in HYPERplan (v. 2.0, Dr. Sennewald Medicine Technique, Munich, Germany) HTP platform (Lang et al., 1999; Gellermann et al., 2000).

2.5. Robustness assessment

For all three perfusion models, we studied the influence of several parameters on the CTV temperature coverage. The comparisons were done by scaling the total HYPERcollar3D input power to achieve 44 °C (or to other maximum allowed temperatures in the range of 42 °C–45 °C) per scenario. We studied the robustness of T50 in the CTV to.

- Blood perfusion (ω)- values for all tissues were scaled in the range of 0.5–1.5 with steps of 0.1. For the temperature dependent model, we changed the values for 37 °C which were for muscle, fat and tumour locally modified using the scaling factor SF shown in Fig. 2.
- Thermal conductivity (k) - values for all tissues were scaled in the range of 0.5–1.5 with steps of 0.1.
- Maximum allowed temperature in healthy tissue ($T_{max,\ healthy}$) - threshold for maximum allowed temperature in healthy tissue was varied in range of 42 °C–45 °C with steps of 0.5 °C.

3. Results

3.1. Temperature cooling modelling

Cumulative T50 temperature histograms for 93 treatments and all three models are shown in Fig. 3. The average of all T50's for the constant model 1 ($\omega_{const.,37°C}$) was equal to 41.0 ± 1.3 °C, for constant model 2 ($\omega_{const.,Tstress}$) 39.9 ± 1.1 °C and for the temperature dependent model ($\omega_{T\text{-}dependent}$) 41.7 ± 1.1 °C. Temperature in critical organs exceed 40 °C in 12/93 cases for $\omega_{const.,Tstress}$ and in 22/93 cases for the $\omega_{T\text{-}dependent}$ models, while for the $\omega_{const.,37°C}$ model all maximum predicted temperatures in critical organs were below 40 °C.

Mean power to obtain maximum temperature of 44 °C for the $\omega_{const.,37°C}$ model was equal to 35.1 ± 9.9 W, for the $\omega_{const.,T\text{-}stress}$ model it was 132.7 ± 45.9 W and for the $\omega_{T\text{-}dependent}$ model it was 59.0 ± 22.2 W. In comparison to the mean power of 129.1 ± 83.0 W applied during HT treatments, the $\omega_{const.,T\text{-}stress}$ model shows the closest predicted power. Fig. 4 shows the predicted mean SAR (W/kg) inside the CTV for all 20

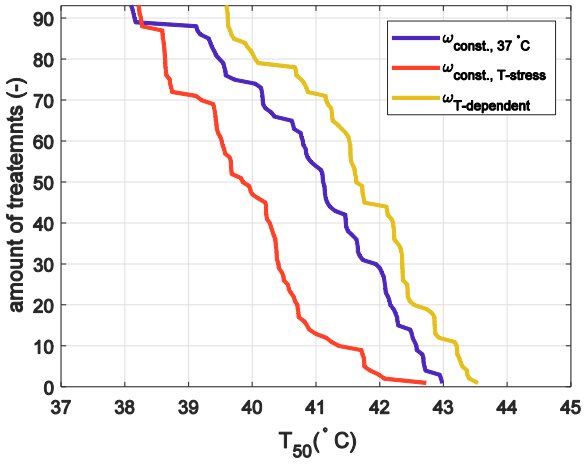

Fig. 3. T50 cumulative histograms from 93 treatments for constant model 1 ($\omega_{const.,37°C}$), constant model 2 developed under temperature stress ($\omega_{const.,T\text{-}stress}$) and temperature dependent ($\omega_{T\text{-}dependent}$) thermal models.

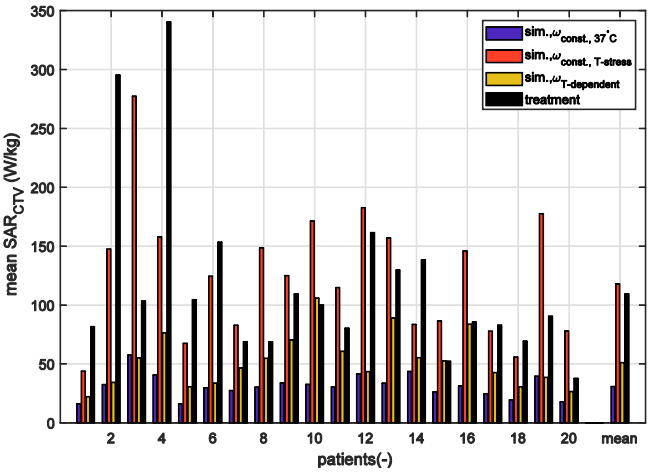

Fig. 4. Mean predicted SAR within the CTV (mean SAR_{CTV}) for 20 patients and for constant literature ($\omega_{const.,37°C}$), constant values under temperature stress ($\omega_{const.,T\text{-}stress}$), temperature dependent ($\omega_{T\text{-}dependent}$) thermal models and power levels applied during the HT treatments.

patients and all three studied temperature models using optimized power levels and mean power applied during HT treatments. Mean simulated SAR for the $\omega_{const.,37°C}$ model was equal to 30.7 ± 10.2 W/kg, for the $\omega_{const.,T\text{-}stress}$ model it was 117.9 ± 54.9 W/kg, for the $\omega_{T\text{-}dependent}$ model it was 51.1 ± 21.0 W/kg and for the HT treatments 109.4 ± 65.7 W/kg.

3.2. Robustness assessment

Fig. 5 a,b,c) and Fig. 5 d,e,f) show robustness assessments of the mean T50 and mean simulated power P (W) as a function of blood perfusion, thermal conductivity and maximum allowed temperature in healthy tissue for all three studied temperature models. The T50 results for $\omega_{const.,37\ °C}$ are almost constant when increasing perfusion (0.12 °C change), while T50 is decreasing for the $\omega_{const.,T\text{-}stress}$ and the $\omega_{T\text{-}dependent}$ models (Fig. 5a). For changes in thermal conductivity, T50 is increasing for all three models Fig. 5b). For both scenarios, the largest changes are for the $\omega_{const.,T\text{-}stress}$ model due to the highest absolute perfusion and thermal conductivity changes. For this model simultaneous increase of blood perfusion and thermal conductivity could result in the same mean T50 (see Fig. 5a and b). When increasing the temperature threshold for healthy tissue ($T_{max.,\ healthy}$) by one degree, the T50 in the target region will increase by 0.65 °C for the $\omega_{const.,37°C}$ model, 0.42 °C for the $\omega_{const.,T\text{-}stress}$ model and 0.75 °C for the $\omega_{T\text{-}dependent}$ model (Fig. 5c).

4. Discussion

For the 20 patient specific head and neck models and 93 treatments with the HYPERcollar3D, we found average T50 differences of 0.7 °C and 1.8 °C, respectively, between two constant ($\omega_{const.,37°C}$ and $\omega_{const.,Tstress}$) and one temperature dependent blood perfusion model ($\omega_{T\text{-}dependent}$). This large impact confirmed our findings from the previous study, where we found T50 differences of on average 1.6 °C for the HYPERcollar (the predecessor of HYPERcollar3D) between the constant heat stress model and the temperature dependent blood perfusion model (Drizdal et al., 2018). As expected, the thermal stress perfusion model performed best out of the three studied models with respect to mean predicted P = 132.7 ± 45.9 W and applied power during the HT P = 129.1 ± 83.0 W. These power levels resulted in predicted SAR levels of 117.9 ± 54.9 W/kg and 109.4 ± 65.7 W/kg respectively, which demonstrates increased SAR delivery using the HYPERcollar3D system in comparison to first generation HYPERcollar, for which the median SAR of 81.8 W/kg was found (Verduijn et al., 2018). However it must be

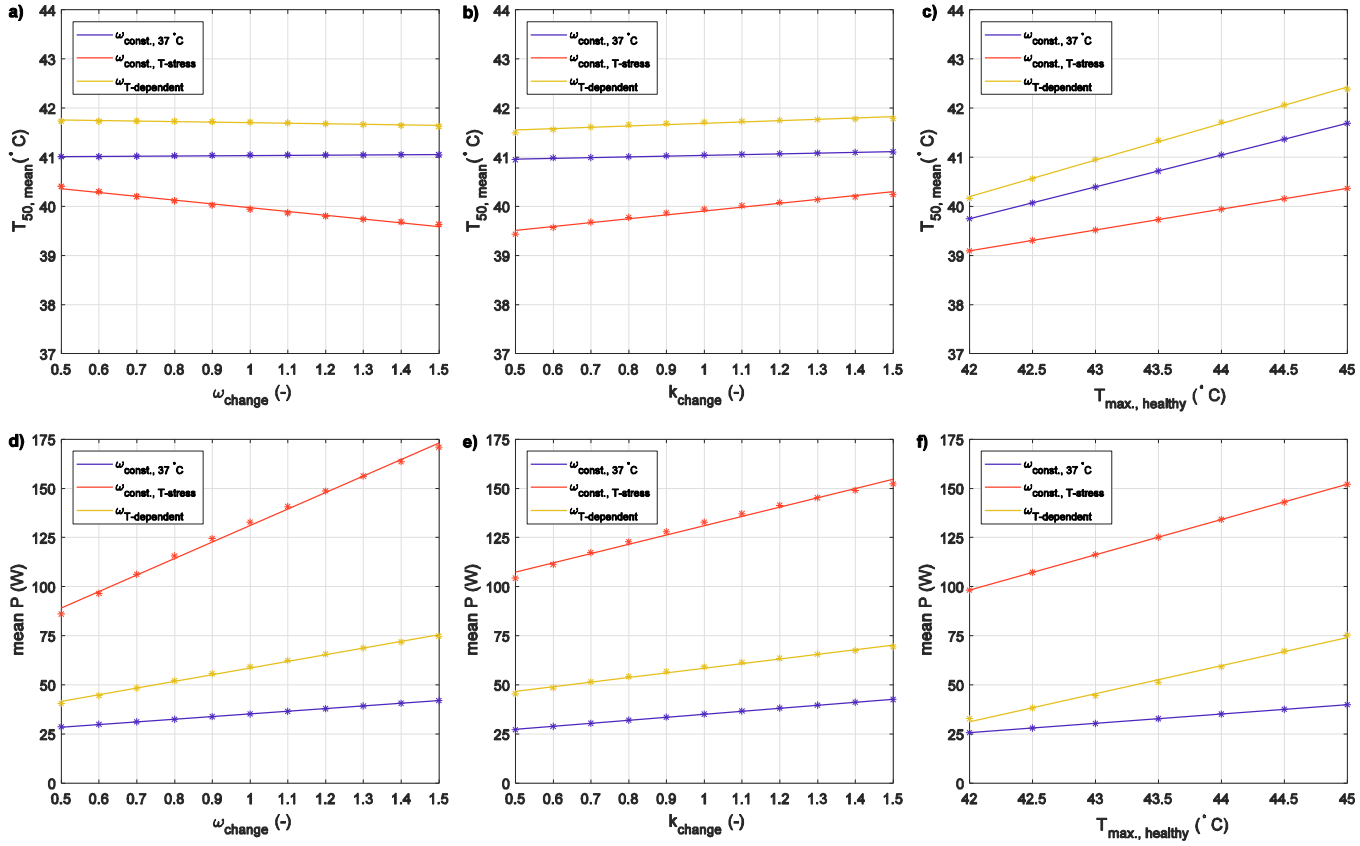

Fig. 5. Influence of changes of blood perfusion, thermal conductivity and maximum allowed temperature during the optimization on T50 (°C) and mean simulated power $P_{sim.}$ (W) for constant literature ($\omega_{const.,37°C}$), constant values under temperature stress ($\omega_{const.,Tstress}$) and temperature dependent ($\omega_{T\text{-}dependent}$) thermal models.

noted that, for this comparison, we assumed to obtain hotspot temperatures of 44 °C in healthy tissue, which is not always guaranteed in clinical practice.

Our results stress the need for future development of thermal tissue models. The first constant temperature model ($\omega_{const.,37°C}$) resulted in low total power of 35.1 ± 9.9 W and SAR of 30.7 ± 10.2 W/kg showing incorrectness of using this model for hyperthermia temperature predictions in the head and neck region. Currently, we consider the heat stress model ($\omega_{const.,Tstress}$) to be the most suitable for temperature prediction and optimization using the HYPERcollar3D applicator. However, even though the temperature dependent model resulted in lower power than the real treatments, possibly since this model is derived from data from treatment of rodents in which tumour perfusion even in steady state is already very high. We still believe that this model, complemented with higher temperature dependent increase curves than shown in Fig. 2, might be a better model for H&N temperature predictions. Due to the number of degrees of freedom in such a model, inferring the thermal tissue parameters per tissue would require much more measurement data then invasive probes can offer. Hence, only reliable magnetic resonance thermometry would provide sufficient information. In addition, also the discrete effects of vessels are not included. This would require to apply discrete vasculature modelling involving inclusion of blood flow in individual vessels (Kok et al., 2013a; Sumser et al., 2019). Even though the feasibility of online DIVA optimization was demonstrated by Kok et al. (2013b), the patient specific DIVA modelling and or optimization in clinical practise is still challenging due to the necessity of development patients specific 3D models including vessel tree.

Our simulations showed a linear relationship between changes in blood perfusion ω, thermal conductivity k and maximum allowed temperature in healthy tissue $T_{max.,healthy}$ and T50 and predicted power P. When hotspots in clinical practice are achieved for a 1 °C higher $T_{max.,healthy}$, the predicted T50 will increase by 0.42 °C for the thermal stress model ($\omega_{const.,Tstress}$), and thus an improved HT quality is predicted. To predict power level of the HT system for obtaining desired temperature of e.g. 43 °C in the target region, requires an absolute SAR prediction of HT systems. Further, use of quantitatively validated systems connected with temperature measurements from the target region would allow to use the agreement between predicted and measured temperatures for reconstruction of tissue temperature parameters, as done by Verhaart et al. (2014a, 2015). Without accurate absolute SAR, non-unique tissue properties are obtained so the reconstructed tissue properties depend on the SAR used and hence are only useful for the respective applicator and not generalizable to other applications, as also found by Verhaart et al. (2014a, 2015). Gellermann et al. (2006) showed agreement of 10% between absolute predicted and measured (using MRI thermometry) SAR in phantoms for MRI compatible version of Sigma Eye, setting up the benchmark for other phase array hyperthermia systems (Winter et al., 2016; Feddersen et al., 2020).

The thermal stress model used for temperature predictions in this study was inferred from temperatures measured during treatment with the previous applicator (the HYPERcollar). The design of the HYPERcollar3D intended to solve a number of clinical limitations of the HYPERcollar, i.e. higher efficiency with higher antennas amount and their optimized placement and separation of the water bolus into two compartments. While the heating performance and SAR control improved, the patch antennas and their orientation in the phased array still provide an equivalent radiation characteristic of the system. Therefore, we expect that the thermal stress model ($\omega_{const.,Tstress}$) also holds for the HYPERcollar3D applicator, but this hypothesis requires confirmation also by temperatures measured during treatment. As explained, placement of invasive thermometry catheters is cumbersome,

represents a burden for the patient and provides temperature information only at several discrete locations. While invasive thermometry was applied in approximately 30% of HYPERcollar treatments (enabling inference of thermal tissue properties), the increasing confidence in the simulations combined with the limitations and risks of invasive thermometry led to a different trade-off for the HYPERcollar3D: i.e. invasive measurements in only three patients (Verduijn et al., 2018; Kroesen et al., 2021). To overcome these limitations, we developed the MRcollar applicator that is compatible with an MRI system to enable non-invasive 3D magnetic resonance thermal imaging (MRTI) during treatment (Drizdal et al., 2021a). The MRTI enables comparison of the 3D measured and predicted temperature distributions for validating and/or improving the temperature heat stress model.

A temperature difference of 0.5 °C was found when comparing the constant literature model ($\omega_{const.,37°C}$) and the temperature dependent model ($\omega_{T\text{-}dependent}$) for HT in the pelvic region (Lang et al., 1999). We assume that the higher difference of 0.7 °C found in this study is caused by the stronger thermoregulation in the head and neck, and the more focussed heating profile of the HYPERcollar3D. Still, it confirms that a higher temperature in the target region will be obtained when applying the temperature dependent blood perfusion model. The constant perfusion values were scaled in several studies following the temperature dependent perfusion in order to compensate for blood perfusion increase (Kumaradas and Sherar, 2003; Kok et al., 2006; der Gaag et al., 2006). Note that these higher constant perfusion values will result in a different power necessary to obtain the maximum temperature in normal tissue with only a small temperature change in the target region: when changing the values by ±50% we found a maximum T50 difference of 0.12 °C for the literature perfusion model (Drizdal et al., 2010).

Applying the temperature stress model ($\omega_{const.,Tstress}$) increases the perfusion and thermal conductivity values also in the regions that are not exposed to heat stress. This could be partly solved by the temperature dependent blood perfusion model, in which perfusion values are only increased in the heated region. A limitation of all models is that they do not model the time dependence of blood perfusion changes, i.e. the organism reacts with certain delay (Guiot et al., 1998). In general, a standardized thermal tissue model is missing, which is mainly due to challenge to obtain “in-vivo” measurements under the heat stress from clinical practise. When this data becomes available, and such models could be inferred, temperature predictions would gain wider acceptance for improving treatment quality and analyses, as well as accelerate technological innovations in developments of improved HT systems and better optimization strategies. Note however that predictive thermal modelling also requires accurate control over the applied SAR, i.e. control over the power and phase of signals applied to the antennas and patient positioning. While control of these parameters is crucial, our study indicates that the appropriate thermal tissue models also strongly affect the predicted temperature.

5. Conclusion

The temperature dependent model predicts an unrealistically high T50, as earlier found also for deep pelvic hyperthermia. The power values for the constant thermal stress model, after scaling simulated normal tissue hotspot temperatures to 44 °C, matched best to the average measured powers. Our study indicates that this model is most suitable for hyperthermia temperature predictions in the H&N region using the HYPERcollar3D applicator. However, further studies are necessary to validate the temperature model for tissues under heat stress in the H&N and other locations.

Authorship statement

Conceptualization: T.D., G.C.v.R., J.V. and M.M.P.; Data curation: T.D., O.F, N. v.H. and M.M.P.; Formal analysis: T.D., D.V., N. v.H. and M.M.P.; Funding acquisition: G.C.v.R. and M.M.P.; Investigation: T.D., G.C.v.R. and M.M.P.; Methodology: T.D., G.C.v.R., J.V. and M.M.P.; Project administration: G.C.v.R. and M.M.P.; Resources: T.D., G.C.v.R., J.V. and M.M.P.; Software: T.D., D. V and O.F; Supervision: G.C.v.R., J.V. and M.M.P.; Validation: T.D., D.V. and O.F.; Visualization: T.D., D.V., O.F.; Roles/Writing - original draft: T.D., G.C.v.R. and M.M.P.; Writing - review & editing: T.D., G.C.v.R., D.V., O.F., N. v.H., J.V. and M.M.P.

Funding sources

This study was developed within the framework of COST Action MyWAVE CA17115 and was supported by the Czech Science Foundation project number 21-00579S and by the Dutch Cancer Society grant EMCR 11368.

Declaration of competing interest

G. C. van Rhoon and M. M. Paulides have financial interest in Sensius BV. All other authors declare no conflict of interest.

References

Bellizzi, G.G., Drizdal, T., van Rhoon, G.C., Crocco, L., Isernia, T., Paulides, M.M., 2019. The potential of constrained SAR focusing for hyperthermia treatment planning: analysis for the head & neck region. Phys. Med. Biol. 64 (1), 015013 https://doi.org/10.1088/1361-6560/aaf0c4.

Canters, R.A.M., Paulides, M.M., Franckena, M.F., van der Zee, J., van Rhoon, G.C., 2012. Implementation of treatment planning in the routine clinical procedure of regional hyperthermia treatment of cervical cancer: an overview and the Rotterdam experience. Int. J. Hyperther. 28 (6), 570–581. https://doi.org/10.3109/02656736.2012.675630.

Cappiello, G., McGinley, B., Elahi, M.A., Drizdal, T., Paulides, M.M., Glavin, M., O'Halloran, M., Jones, E., 2017. Differential evolution optimization of the SAR distribution for head and neck hyperthermia. IEEE (Inst. Electr. Electron. Eng.) Trans. Biomed. Eng. 64 (8), 1875–1885. https://doi.org/10.1109/TBME.2016.2627941.

Chen, S., 2016. Particle swarm optimization toolbox version 20130702, Technical report. http://www.mathworks.com/matlabcentral/fileexchange/25986.

de Greef, M., Kok, H.P., Correia, D., Bel, A., Crezee, J., 2010. Optimization in hyperthermia treatment planning: the impact of tissue perfusion uncertainty. Med. Phys. 37 (9), 4540–4550. https://doi.org/10.1118/1.3462561.

de Greef, M., Kok, H.P., Correia, D., Borsboom, P.-P., Bel, A., Crezee, J., 2011. Uncertainty in hyperthermia treatment planning: the need for robust system design. Phys. Med. Biol. 56, 3233–3250. https://doi.org/10.1088/0031-9155/56/11/005.

der Gaag, M.L.V., de Bruijne, M., Samaras, T., van der Zee, J., van Rhoon, G.C., 2006. Development of a guideline for the water bolus temperature in superficial hyperthermia. Int. J. Hyperther. 22 (8), 637–656. https://doi.org/10.1080/02656730601074409.

Drizdal, T., Togni, P., Visek, L., Vrba, J., 2010. Comparison of constant and temperature dependent blood perfusion in temperature prediction for superficial hyperthermia. Radioengineering 19 (2), 281–289. https://www.radioeng.cz/fulltexts/2010/10_02_281_289.pdf.

Drizdal, T., Paulides, M.M., van Holthe, N., van Rhoon, G.C., 2018. Hyperthermia treatment planning guided applicator selection for sub-superficial head and neck tumors heating. Int. J. Hyperther. 34, 704–713. https://doi.org/10.1080/02656736.2017.1383517.

Drizdal, T., Sumser, K., Bellizzi, G.G., Fiser, O., Vrba, J., Rhoon, G.C.v., Yeo, D.T.B., Paulides, M.M., 2021a. Simulation guided design of the MRcollar: a MR compatible applicator for deep heating in the head and neck region. Int. J. Hyperther. 38, 382–392. https://doi.org/10.1080/02656736.2021.1892836.

Drizdal, T., van Rhoon, G.C., Verhaart, R.F., Fiser, O., Paulides, M.M., 2021b. A guide for water bolus temperature selection for semi-deep head and neck hyperthermia treatments using the HYPERcollar3D applicator. Cancers 13. https://doi.org/10.3390/cancers13236126.

Feddersen, T.V., Hernandez-Tamames, J.A., Franckena, M., van Rhoon, G.C., Paulides, M.M., 2020. Clinical performance and future potential of magnetic resonance thermometry in hyperthermia. Cancers 13 (1), 31. https://doi.org/10.3390/cancers13010031.

Franckena, M., Stalpers, L.J.A., Koper, P.C.M., Wiggenraad, R.G.J., Hoogenraad, W.J., van Dijk, J.D.P., Wárlám-Rodenhuis, C.C., Jobsen, J.J., van Rhoon, G.C., van der Zee, J., 2008. Long-term improvement in treatment outcome after radiotherapy and hyperthermia in locoregionally advanced cervix cancer: an update of the Dutch Deep Hyperthermia Trial. Int. J. Radiat. Oncol. Biol. Phys. 70 (4), 1176–1182. https://doi.org/10.1016/j.ijrobp.2007.07.2348.

Gabriel, S., Lau, R.W., Gabriel, C., 1996. The dielectric properties of biological tissues: III. Parametric models for the dielectric spectrum of tissues. Phys. Med. Biol. 41 (11), 2271–2293. https://doi.org/10.1088/0031-9155/41/11/003.

Gaffoglio, R., Righero, M., Giordanengo, G., Zucchi, M., Vecchi, G., 2021. Fast optimization of temperature focusing in hyperthermia treatment of sub-superficial tumors. IEEE Journal of Electromagnetics, RF and Microwaves in Medicine and Biology 5 (3), 286–293. https://doi.org/10.1109/JERM.2020.3043383.

Gavazzi, S., van Lier, A.L.H.M.W., Zachiu, C., Jansen, E., Lagendijk, J.J.W., Stalpers, L.J. A., Crezee, H., Kok, H.P., 2020. Advanced patient-specific hyperthermia treatment planning. Int. J. Hyperther. 37, 992–1007. https://doi.org/10.1080/02656736.2020.1806361.

Gellermann, J., Weihrauch, M., Cho, C.H., Wlodarczyk, W., Fähling, H., Felix, R., Budach, V., Weiser, M., Nadobny, J., Wust, P., 2006. Comparison of MR-thermography and planning calculations in phantoms. Med. Phys. 33, 3912–3920. https://doi.org/10.1118/1.2348761.

Gellermann, J., Wust, P., Stalling, D., Seebass, M., Nadobny, J., Beck, R., Hege, H., Deuflhard, P., Felix, R., 2000. Clinical evaluation and verification of the hyperthermia treatment planning system hyperplan. Int. J. Radiat. Oncol. Biol. Phys. 47, 1145–1156. https://doi.org/10.1016/s0360-3016(00)00425-9.

Guiot, C., Madon, E., Allegro, D., Piantà, P.G., Baiotto, B., Gabriele, P., 1998. Perfusion and thermal field during hyperthermia. experimental measurements and modelling in recurrent breast cancer. Phys. Med. Biol. 43, 2831–2843. https://doi.org/10.1088/0031-9155/43/10/012.

Hasgall, P., Gennaro, F.D., Baumgartner, C., Neufeld, E., Lloyd, B., Gosselin, M., Payne, D., Klingenböck, A., Kuster, N., 2018. ITIS database for thermal and electromagnetic parameters of biological tissues. www.itis.ethz.ch/database.

Issels, R.D., Lindner, L.H., Verweij, J., Wessalowski, R., Reichardt, P., Wust, P., Ghadjar, P., Hohenberger, P., Angele, M., Salat, C., Vujaskovic, Z., Daugaard, S., Mella, O., Mansmann, U., Dürr, H.R., Knösel, T., Abdel-Rahman, S., Schmidt, M., Hiddemann, W., Jauch, K.-W., Belka, C., Gronchi, A., 2018. Effect of neoadjuvant chemotherapy plus regional hyperthermia on long-term outcomes among patients with localized high-risk soft tissue sarcoma: the EORTC 62961-ESHO 95 randomized clinical trial. JAMA Oncol. 4, 483–492. https://doi.org/10.1001/jamaoncol.2017.4996.

Kok, H.P., van Haaren, P.M.A., van de Kamer, J.B., Zum Vörde Sive Vörding, P.J., Wiersma, J., Hulshof, M.C.C.M., Geijsen, E.D., van Lanschot, J.J.B., Crezee, J., 2006. Prospective treatment planning to improve locoregional hyperthermia for oesophageal cancer. Int. J. Hyperther. 22, 375–389. https://doi.org/10.1080/02656730600760149.

Kok, H.P., Gellermann, J., van den Berg, C.A.T., Stauffer, P.R., Hand, J.W., Crezee, J., 2013a. Thermal modelling using discrete vasculature for thermal therapy: a review. Int. J. Hyperther. 29, 336–345. https://doi.org/10.3109/02656736.2013.801521.

Kok, H.P., van den Berg, C.A.T., Bel, A., Crezee, J., 2013b. Fast thermal simulations and temperature optimization for hyperthermia treatment planning, including realistic 3D vessel networks. Med. Phys. 40, 103303 https://doi.org/10.1118/1.4821544.

Kok, H.P., Korshuize-van Straten, L., Bakker, A., de Kroon-Oldenhof, R., Westerveld, G. H., Versteijne, E., Stalpers, L.J.A., Crezee, J., 2017. Feasibility of on-line temperature-based hyperthermia treatment planning to improve tumour temperatures during locoregional hyperthermia. Int. J. Hyperther. 34, 1082–1091. https://doi.org/10.1080/02656736.2017.1400120.

Kok, H.P., Cressman, E.N.K., Ceelen, W., Brace, C.L., Ivkov, R., Grüll, H., Ter Haar, G., Wust, P., Crezee, J., 2020. Heating technology for malignant tumors: a review. Int. J. Hyperther. 37, 711–741. https://doi.org/10.1080/02656736.2020.1779357.

Kok, H.P., Crezee, J., 2021. Hyperthermia treatment planning: clinical application and ongoing developments. IEEE Journal of Electromagnetics, RF and Microwaves in Medicine and Biology 5 (3), 214–222. https://doi.org/10.1109/JERM.2020.3032838.

Kok, H.P., van der Zee, J., Guirado, F.N., Bakker, A., Datta, N.R., Abdel-Rahman, S., Schmidt, M., Wust, P., Crezee, J., 2021b. Treatment planning facilitates clinical decision making for hyperthermia treatments. Int. J. Hyperther. 38, 532–551. https://doi.org/10.1080/02656736.2021.1903583.

Kroesen, M., van Holthe, N., Sumser, K., Chitu, D., Vernhout, R., Verduijn, G., Franckena, M., Hardillo, J., van Rhoon, G., Paulides, M., 2021. Feasibility, SAR distribution, and clinical outcome upon reirradiation and deep hyperthermia using the HYPERcollar3D in head and neck cancer patients. Cancers 13. https://doi.org/10.3390/cancers13236149.

Kumaradas, J.C., Sherar, M.D., 2003. Edge-element based finite element analysis of microwave hyperthermia treatments for superficial tumours on the chest wall. Int. J. Hyperther. 19, 414–430. https://doi.org/10.1080/0265673031000074457.

Lang, J., Erdmann, B., Seebass, M., 1999. Impact of nonlinear heat transfer on temperature control in regional hyperthermia. IEEE (Inst. Electr. Electron. Eng.) Trans. Biomed. Eng. 46 (9), 1129–1138. https://doi.org/10.1109/10.784145.

Paulides, M.M., Stauffer, P.R., Neufeld, E., Maccarini, P.F., Kyriakou, A., Canters, R.A.M., Diederich, C.J., Bakker, J.F., Van Rhoon, G.C., 2013. Simulation techniques in hyperthermia treatment planning. Int. J. Hyperther. 29 (4), 346–357. https://doi.org/10.3109/02656736.2013.790092.

Paulides, M.M., Verduijn, G.M., Van Holthe, N., 2016. Status quo and directions in deep head and neck hyperthermia. Radiat. Oncol. 11 (1), 21. https://doi.org/10.1186/s13014-016-0588-8.

Peeters, H., van Zwol, E.M., Brancato, L., Cunha, M.G., Bogers, J., 2022. Systematic review of the registered clinical trials for oncological hyperthermia treatment. Int. J. Hyperther. 39, 806–812. https://doi.org/10.1080/02656736.2022.2076292.

Pennes, H.H., 1948. Analysis of tissue and arterial blood temperatures in the resting human forearm. J. Appl. Physiol. 1 (2), 93–122. https://doi.org/10.1152/jappl.1998.85.1.5.

Rijnen, Z., Bakker, J.F., Canters, R.A.M., Togni, P., Verduijn, G.M., Levendag, P.C., Van Rhoon, G.C., Paulides, M.M., 2013. Clinical integration of software tool VEDO for adaptive and quantitative application of phased array hyperthermia in the head and neck. Int. J. Hyperther. 29 (3), 181–193. https://doi.org/10.3109/02656736.2013.783934.

Song, C.W., Lokshina, A., Rhee, J.G., Patten, M., Levitt, S.H., 1984. Implication of blood flow in hyperthermic treatment of tumors. IEEE (Inst. Electr. Electron. Eng.) Trans. Biomed. Eng. 31 (1), 9–16. https://doi.org/10.1109/TBME.1984.325364. BME-.

Sumser, K., Neufeld, E., Verhaart, R.F., Fortunati, V., Verduijn, G.M., Drizdal, T., van Walsum, T., Veenland, J.F., Paulides, M.M., 2019. Feasibility and relevance of discrete vasculature modeling in routine hyperthermia treatment planning. Int. J. Hyperther. 36, 801–811. https://doi.org/10.1080/02656736.2019.1641633.

Togni, P., Rijnen, Z., Numan, W.C.M., Verhaart, R.F., Bakker, J.F., van Rhoon, G.C., Paulides, M.M., 2013. Electromagnetic redesign of the HYPERcollar applicator: toward improved deep local head-and-neck hyperthermia. Phys. Med. Biol. 58 (17), 5997–6009. https://doi.org/10.1088/0031-9155/58/17/5997.

Verduijn, G.M., de Wee, E.M., Rijnen, Z., Togni, P., Hardillo, J.A.U., Ten Hove, I., Franckena, M., van Rhoon, G.C., Paulides, M.M., 2018. Deep hyperthermia with the HYPERcollar system combined with irradiation for advanced head and neck carcinoma - a feasibility study. Int. J. Hyperther. 34, 994–1001. https://doi.org/10.1080/02656736.2018.1454610.

Verhaart, R.F., Rijnen, Z., Fortunati, V., Verduijn, G.M., van Walsum, T., Veenland, J.F., Paulides, M.M., 2014a. Temperature simulations in hyperthermia treatment planning of the head and neck region: rigorous optimization of tissue properties. Strahlenther. Onkol. 190 (12), 1117–1124. https://doi.org/10.1007/s00066-014-0709-y.

Verhaart, R.F., Fortunati, V., Verduijn, G.M., van Walsum, T., Veenland, J.F., Paulides, M.M., 2014b. CT-based patient modeling for head and neck hyperthermia treatment planning: manual versus automatic normal-tissue-segmentation. Radiother. Oncol. 111 (1), 158–163. https://doi.org/10.1016/j.radonc.2014.01.027.

Verhaart, R.F., Verduijn, G.M., Fortunati, V., Rijnen, Z., van Walsum, T., Veenland, J.F., Paulides, M.M., 2015. Accurate 3D temperature dosimetry during hyperthermia therapy by combining invasive measurements and patient-specific simulations. Int. J. Hyperther. 31 (6), 686–692. https://doi.org/10.3109/02656736.2015.1052855.

Winter, L., Oberacker, E., Paul, K., Ji, Y., Oezerdem, C., Ghadjar, P., Thieme, A., Budach, V., Wust, P., Niendorf, T., 2016. Magnetic resonance thermometry: methodology, pitfalls and practical solutions. Int. J. Hyperther. 32 (1), 63–75. https://doi.org/10.3109/02656736.2015.1108462.

Glossary

T50 (°C): median target temperature
SAR (W kg^{-1}): specific absorption rate
P (W): power
CT: computed tomography
CTV: clinical target volume
EM: electromagnetic
HT: hyperthermia treatment
HTP: hyperthermia treatment planning
H&N: head and neck
VEDO: visualization tool for electromagnetic dosimetry and optimization